Fernández, E. M. *et al.,* 2007. Massive sulphides search at the Iberian Pyrite Belt: petrophysical data, geophysical natural fields and mineral favourability mapping. *Boletín Geológico y Minero,* 118 (1): 19-36
ISSN: 0366-0176

Massive sulphides search at the Iberian Pyrite Belt: petrophysical data, geophysical natural fields and mineral favourability mapping

E.M. Fernández, J.L. García-Lobón and C. Ayala

Instituto Geológico y Minero de España. Ríos Rosas, 23. 28003 Madrid
evamarff@gmail.com, jl.garcia@igme.es, c.ayala@igme.es

ABSTRACT

In this study we describe an application of several algorithms for mineral favourability mapping in a well-known metallogenic province, the Iberian Pyrite Belt. We have processed and interpreted some available high resolution geophysical coverages (ground gravity and airborne magnetic and radiometric data), and related them to surface geology, to detailed structural maps, and to the occurrence of the Pyrite Belt ore deposits. We also analyse the variation of petrophysical properties (rock density, magnetic susceptibility, remanent magnetization, and natural gamma radiation) measured in field and laboratory from surface rocks at the Northwestern Domain of the Belt, and describe the relationship of these properties with the available regional geophysical data as well as their significance for massive sulphide exploration in the Belt. Using all the aforementioned information, a test of several integrated GIS-based data driven classifiers has been run. These tools generate mineral favourability images using several mapping function algorithms (neural network, weights of evidence, and logistic regression methods). Mineral favourability maps allow areal evaluation and definition of possible massive sulphide occurrences, suitable for developing new mining prospects. The utility of petrophysical data and regional natural-field geophysical images for subsurface mapping and deposit search is discussed, and some useful indications on the statistical integration of geophysical potential field images with surface geology, structure and mineral occurrences are extracted.

Key words: geophysical natural fields, Iberian Pyrite Belt, mineral favourability mapping, petrophysics

Búsqueda de depósitos de sulfuros masivos en la Faja Pirítica: petrofísica, imágenes geofísicas de campo natural y mapas de favorabilidad minera

RESUMEN

En este trabajo describimos la aplicación de diversos algoritmos de generación de mapas de favorabilidad minera en una provincia metalogénica bien conocida: la Faja Pirítica Ibérica. Hemos procesado e interpretado las coberturas geofísicas de alta resolución disponibles en la zona (datos gravimétricos terrestres y datos de magnetometría y radiometría aeroportadas de alta resolución), estableciéndose su correlación con la geología de superficie, mapas estructurales detallados y depósitos minerales de la Faja Pirítica. También hemos analizado la variación de las propiedades petrofísicas (densidad, susceptibilidad magnética, magnetización remanente y radiación gamma natural) medidas en campo y en laboratorio de las rocas del Dominio Noroeste de la Faja, describiendo la relación entre dichas propiedades y los datos geofísicos disponibles así como su importancia en la exploración de depósitos de sulfuros masivos. Utilizando toda la información mencionada, hemos llevado a cabo un ensayo con varios algoritmos de clasificación implementados en SIG. Mediante estas herramientas, hemos generado mapas de favorabilidad minera utilizando los métodos de redes neuronales, pesos de las evidencias y regresión logística. Los mapas de favorabilidad minera permiten la evaluación areal y la definición de la posible localización de nuevos depósitos de sulfuros masivos. Discutimos la utilidad de los datos petrofísicos y las imágenes geofísicas de campo natural para la cartografía de subsuelo y la búsqueda de recursos minerales y proporcionamos indicaciones útiles acerca de la integración estadística de los mapas de campo potencial con la geología de superficie, los mapas estructurales y los depósitos minerales.

Palabras clave: campos geofísicos naturales, Faja Pirítica Ibérica, mapas de favorabilidad minera, petrofísica

Introduction. Geological setting

The Iberian Pyrite Belt (IPB, SW Spain) is one of the largest and most important metallogenic provinces in the world with more than twenty centuries of mining activity (Leistel *et al.,* 1997; Gumiel and Mirete, 1999). The area has been extensively explored for volcanogenic massive sulphide deposits (VMS) and a complete data coverage is available, including high resolution ground gravity and airborne magnetic and radiometric surveys carried out by IGME (Geological Survey of Spain), in the last decade (Bates and García Lobón, 1998).

Recently, IGME has been involved in several integrated projects aimed to improve the geological interpretation of high-resolution magnetic and radiome-

tric airborne data. Petrophysical characterisation of VMS sites sets up the basis for processing and analysing radiometric and potential field images with the purpose of building up geophysical documents for guiding mining prospecting. This guiding is improved by the integration of all these datasets in the framework of GIS algorithmic tools.

The IPB is the northern segment of the South Portuguese Terrane (southwesternmost corner of the Variscan Iberian Massif). The oldest lithologies appear in the North and the youngest in the South, reflecting the thin-skinned south-verging tectonics of the Belt. The geological record exposed in the Northwestern Domain of IPB includes (Leistel y otros and references therein):

(1) Late Devonian marine platformal sequences consisting of quartzites, greywackes and slates. They crop out in the Gafo Unit and the so-called PQ group of Duque Unit (Figure 1.)

(2) A Lower Carboniferous Volcano-Sedimentary Complex (VSC), representing a transtensional and collapse stage. In most structural units (Gibraltar-Panera, Concepción and the SE part of Río Tinto Units in topographic map sheet 937, Figure 1), volcanic materials are predominantly basaltic and rhyolitic, with andesites, pyroclastites and lava flows.

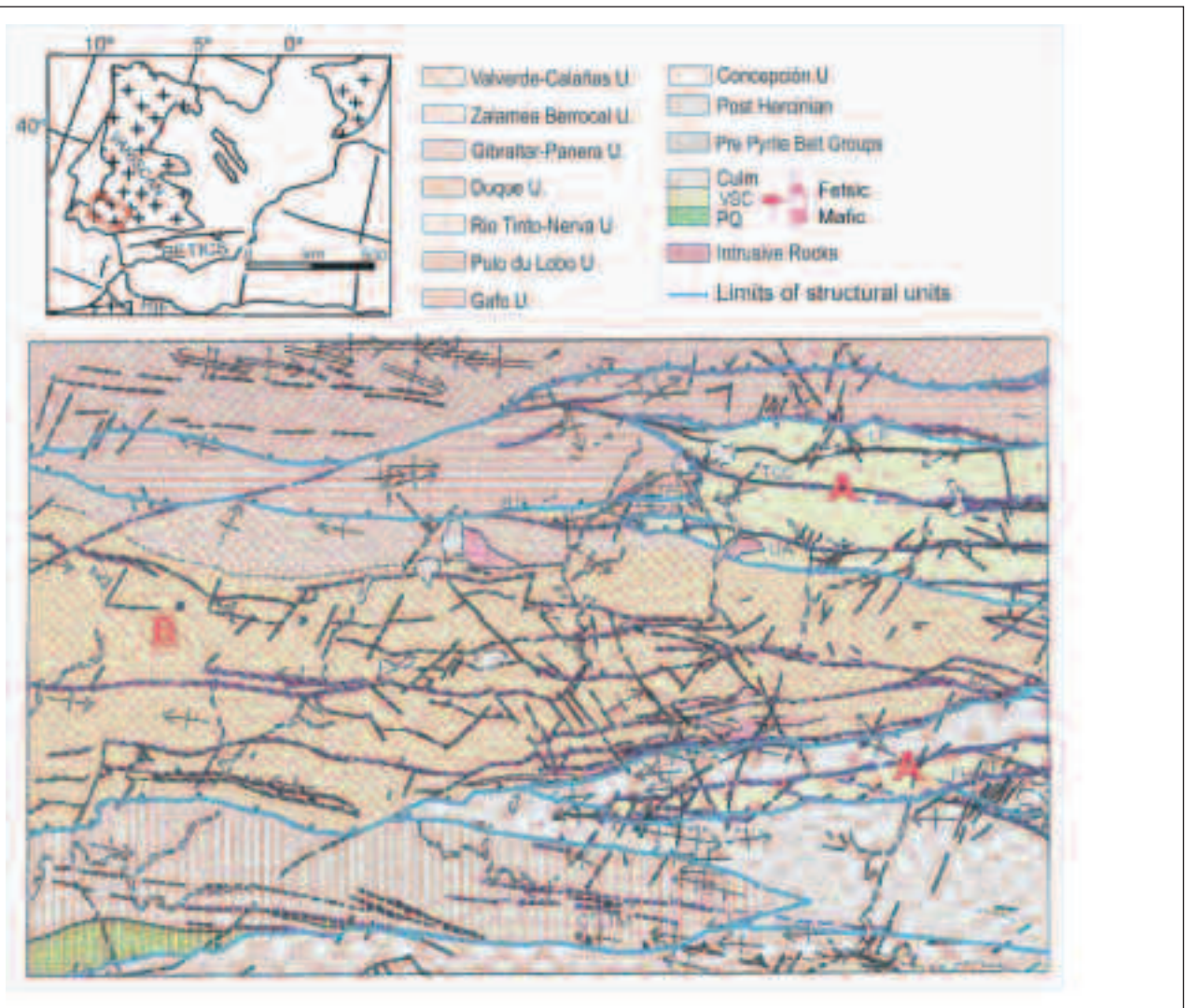

Figure 1. Geological map of the study area (approximate location: red rectangle on the upper left corner map). Modified from the geological map of the Junta de Andalucía (2002)

Figura 1. Mapa geológico del área de estudio (localización aproximada: rectángulo rojo en el mapa de la esquina superior izquierda). Modificado del publicado por la Junta de Andalucía (2002)

Volcanites are interstratified in a pelite-black shale and sandstone sequence, which contains beds of jasper; and,

(3) A Middle-Upper Carboniferous thick turbidite formations of greywackes and slates, known as Culm group, outcropping in the rest of the units of the study area.

It will be shown that tectonic units (Figure 1) and the main structural limits are of great importance for geophysical interpretation and orebody searching. The massive sulphides are hosted by the VSC sequence, either directly in the black shale, or resting on acidic volcanic facies albeit commonly separated by a thin pelitic layer. The mineralization model is of VMS type, genetically related to submarine volcanic activity. Main metallic ores are copper, lead and zinc; gold and silver appear as accessories.

Petrophysical measurements and results

Results of laboratory (rock density, magnetic susceptibility and remanent magnetization) and in-situ ground natural gamma radiation measurements are presented in Table I and Figure 2.

Measurements of density have been made on hammer-cut samples (0.3-0.6 kg) by weighing them in air and water (Archimedes principle). These samples come from 4-5 kg of rock collected in the field. From each of these samples, powder (2 mm grid pass) is obtained and magnetic susceptibility determined in a kappabridge (KLY-2 instrument of AGICO); the mass of the powder is measured, and the kappabridge values are converted to a mass susceptibility, then multiplied by the density of the sample to obtain volume susceptibility. Finally, non-oriented 2-inches prisms are cut and rock remanent magnetization is measured in a spin magnetometer (JR5, also of AGICO). Sensitivities are of the order of 0.01 g/cm^3, 2*10^{-7} cgs units, and 3 *10^{-6} A/m, respectively. Precisions are 0.02 g/cm^3 for density, and better than 5% for the magnetic measurements. A hand-held 256-channel gamma ray spectrometer GR-320 (Exploranium, 1998) has been used to measure concentrations of the natural radioelements potassium, uranium and thorium at the sampling sites. A reference isotopic source avoids shifts in the spectral alignment of the instrument. The measured spectra recorded at each site are processed with the instrument calibration parameters providing the contents

Lithologies	k_{md}	d_{md}	K_{md}	U_{md}	Th_{md}	Q_{mn}
Andesites	45	2.81	0.6	0.6-1.4	6.0	0.13
Basalts	70-1300-3200	2.89	0.4-2.0	0.6	6.0	0.41
Diabases	60-1200	2.95	0.6	-	3.5	0.24
Dacites	30	2.73	1.0-1.4-2.6	1.3	7.0-9.0	0.22
Rhyolites	40-1100	2.59	2.0-3.3-4.9	1.7-3.1	13.0	1.25
Acid tuffs	20	2.55	2.1-3.1	2.2	14.0	0.26
Intermediate tuffs	30-400	2.71	1.0-1.6	1.1	9.0	-
Jaspers	100-1500-5600	2.80	0.2	0.4	1.0-4.0	3.23
Quartzites	37	2.59	-	-	-	-
Sandstones	27	2.60	0.8	-	10.0	-
Greywackes	19	2.53	2.6	2.6	12.0-16.5	0.32
Slates	28	2.37-2.55	3.2	3.1	16.5	0.08
Schists	27	2.53	3.5	3.3	17.0-21.0	0.39

Table I. Modes of magnetic susceptibility k (ucgs*10^6), density d (g/cm^3), and radiometric content of K (%), U (ppm) and Th (ppm). Q_{mn}: Koenigsberger parameter (median)

*Tabla I. Modas de susceptibilidad magnética k (ucgs*10^6), densidad (g/cm^3), y contenido radiométrico en K (%), U (ppm) y Th (PPM). Q_{mn}: parámetro de Koenigsberger (media)*

of potassium, uranium and thorium (%K, ppmU and ppmTh). In situ radiometric estimates of K, U and Th can be expected to correlate well with the actual proportions in the rock sample, if the outcrop offers good measurement conditions (fresh rock, locally flat geometry; Chiozzi *et al.,* 1998).

The results can be summarized as follows (García-Lobón and Ayala, 2004):

1) Volcanic rocks of IPB show a wide range of radioactivities and densities from felsic to mafic terms, and a typical bimodal (or even polymodal) susceptibility distribution in both groups, felsic and mafic volcanics, delineating two well defined trends, either paramagnetic ($k<200*10^{-6}$ ucgs) or ferromagnetic ($k>500*10^{-6}$ ucgs, Figure 2). Bimodality and range overlapping is also typical of radioelement contents (Figure 2). This fact does not facilitate radiometric interpretations, making ground measurements an unavoidable task.

2) Andesites, basalts and diabases show increasing densities, being the source of regional gravity anomalies (caused by Andesitic Formations), which include important maxima (due to imbricated basaltic sills within the Andesitic Fms). Andesites are clearly paramagnetic rocks, while most diabases and basalts are ferromagnetic with modes that represent 0.5-1.2% Fe_3O_4 contents. Spilitic basalts are more consistently ferromagnetic than diabases: both lithologies are abundant, show close relationships and constitute the main gravity and magnetic markers of the IPB. These markers usually mask the responses of local sources that could be attributed to the VMS ore deposits.

3) Felsic volcanics of the NW Domain of IPB, mainly acid tuffs and dacites, are low density paramagnetic rocks. Dacites are petrophysically similar to andesites, being also totally paramagnetic. In the magnetic map, the anomalies displayed by Andesitic-Dacitic formations are due to basaltic sills intercalated within them. Rhyolites and acid tuffs are near paramagnetic rocks, with a subtle trend towards bimodality of susceptibility. In fact, there is a black facies of rhyolites that are moderately ferromagnetic (up to 0.4% of Fe_3O_4).

Figure 2. Density-magnetic susceptibilty (left) and potassium-thorium (right) crossplots
Figura 2. Diagramas bivariantes densidad-susceptibilidad magnética (izquierda) y potasio-torio (derecha)

4) Average densities and susceptibilities of sandstones, greywackes, quartzites, schists and slates range between 2.49-2.57 g/cm^3 and 19-37*10^{-6} ucgs. As felsic volcanics, metasedimentary rocks have low densities and susceptibilities, which do not cause magnetic or gravity anomalies. Jaspers are dense and ferromagnetic, and frequently produce short wavelength magnetic anomalies that constitute an indirect guide for ore body searching in many areas of IPB.

5) Remanence measurements indicate that multidomain magnetite is the main ferromagnetic mineral in basalts and diabases (1.000<k<10.000*10^{-6} ucgs, Q≅0.5). In general, magnetic induction dominates over remanent magnetization, with Koenigsberger ratios Q characteristic of a normal orientated viscous remanence, the exception being jaspers and some rhyolites (the black facies ferromagnetic set). No k-Q values typical of pyrrhotite bearing rocks have been detected in the dataset.

6) Mafic and intermediate volcanics show weak radioactivities (Figure 2). Bimodality of radiometric contents reflects the occurrence of alterations (e.g., potassification of plagioclase and mafic minerals) that confer higher radioactivities to these rocks.

Concerning the felsic terms, typical dacites (1.3<%K<2.8), acid tuffs, and rhyolites of K< 5%, display increasing radioactivity within a common K-Th trend that reflects their genetic relationship. Rhyolites are nearly always easily discernible from dacites.

Dacites appear on low radioactivity areas in the ternary airborne radiometric map, similar to those occurring over andesites, so it is usually not possible to differentiate dacites from andesites in Andesitic-Dacitic Formations. Rhyolites are the most radioactive volcanic rocks, showing great heterogeneity, with several modes in their radioelement histograms. Although acid tuffs radioactivity on the ground data tends to be high, there are wide areas of these rocks on the geological maps with low-moderate emissions in the radiometric images.

7) As acid volcanics, metasedimentary rocks dis-

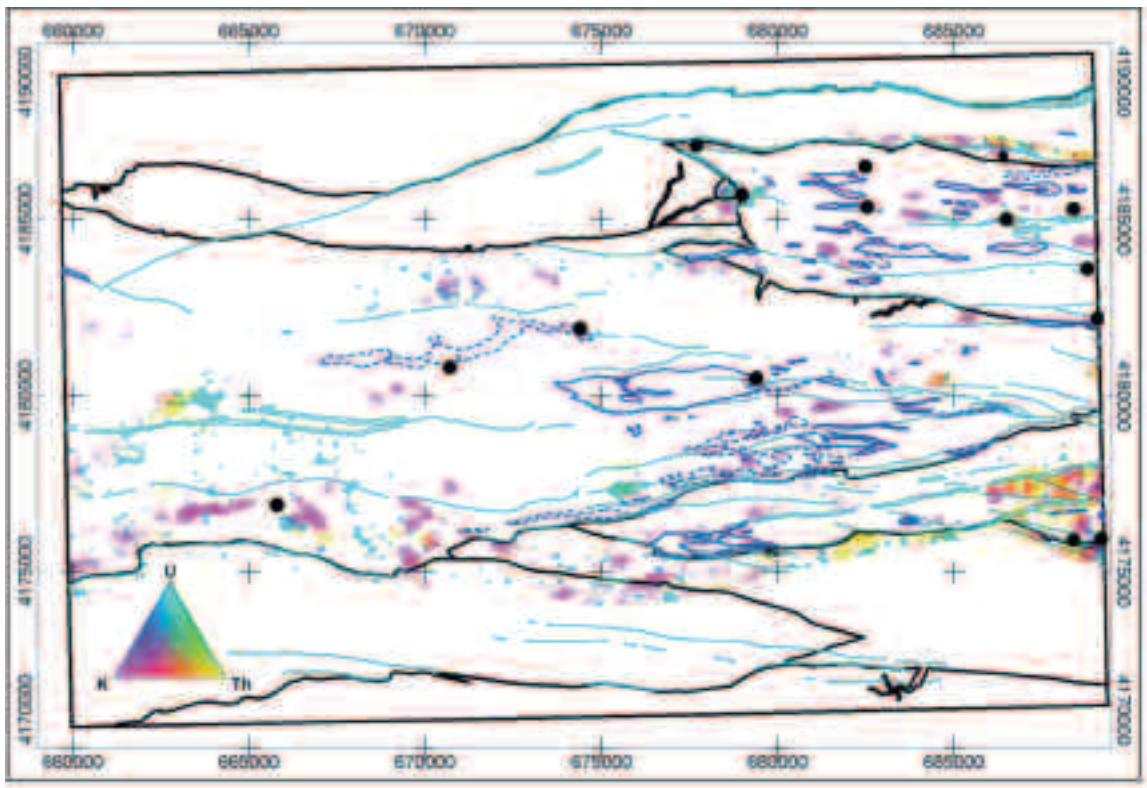

Figure 3. Radiometric Maximum Ternary Map (K > 3.80%, U > 2.80 ppm, Th > 16.49 ppm). Black lines: main tectonic units. Cyan lines: shear bands. Black dots: massive sulphide deposits

Figura 3. Mapa ternario de máximos radiométricos (K > 3.80%, U > 2.80 ppm, Th > 16.49 ppm). Líneas en negro: principales unidades tectónicas. Líneas azules: volcanitas básicas. Líneas cyan: bandas de cizalla. Círculos negros: depósitos de sulfuros masivos

play a wide spectrum of radiometric values, showing increasing radioactivites from sandstones to schists, through greywackes and slates. Radioactive histograms of greywackes suggest a tendency to bimodality, with a group of intermediate radioactivity, similar to sandstones, and another more radioactive, similar to slates. Slates and schists are the most radioactive rocks of the NW Domain of IPB, displaying strong radiometric contrasts with the volcanic set in airborne maps.

8) An outstanding feature of ground radiometric data refers to extreme values, very well separated in the K-Th diagram (K>6%, Figure 2). In particular, spectacular potassifications occur in rhyolites and acid tuffs located close to thrust limits and shear zones, that clearly control them, at least in the felsic volcanic Units (Figure 3). These potassifications constitute a good guide for prospecting VMS deposits. A remarkable fact depicted in Figure 3 is the general low radioactive level of the studied area.

Geophysical images

Bouguer anomalies of the Northwestern Domain of IPB are dominated by a broad regional gradient NW-SE caused by crustal structures that extend across the whole Iberian Pyrite Belt; alternate bands of relative E-W minima/maxima are superimposed over this broad regional gradient. This banding is clearly displayed in the residual Bouguer anomaly image (Figure 4): positive gravity anomalies reflect the occurrence of dense rocks of Andesitic Formations and their imbrications with basaltic lithologies, while sources of negative anomalies are low density felsic volcanites and metasedimentary rocks. As these lithological changes are controlled by the main structural divisions of the studied area, the limits and internal structure of the main tectonic units are very well mapped by gravity residual anomalies. Minima are dominant over the VSC felsic rocks of Concepción, Río Tinto-Nerva and SW of Gibraltar-Panera Units,

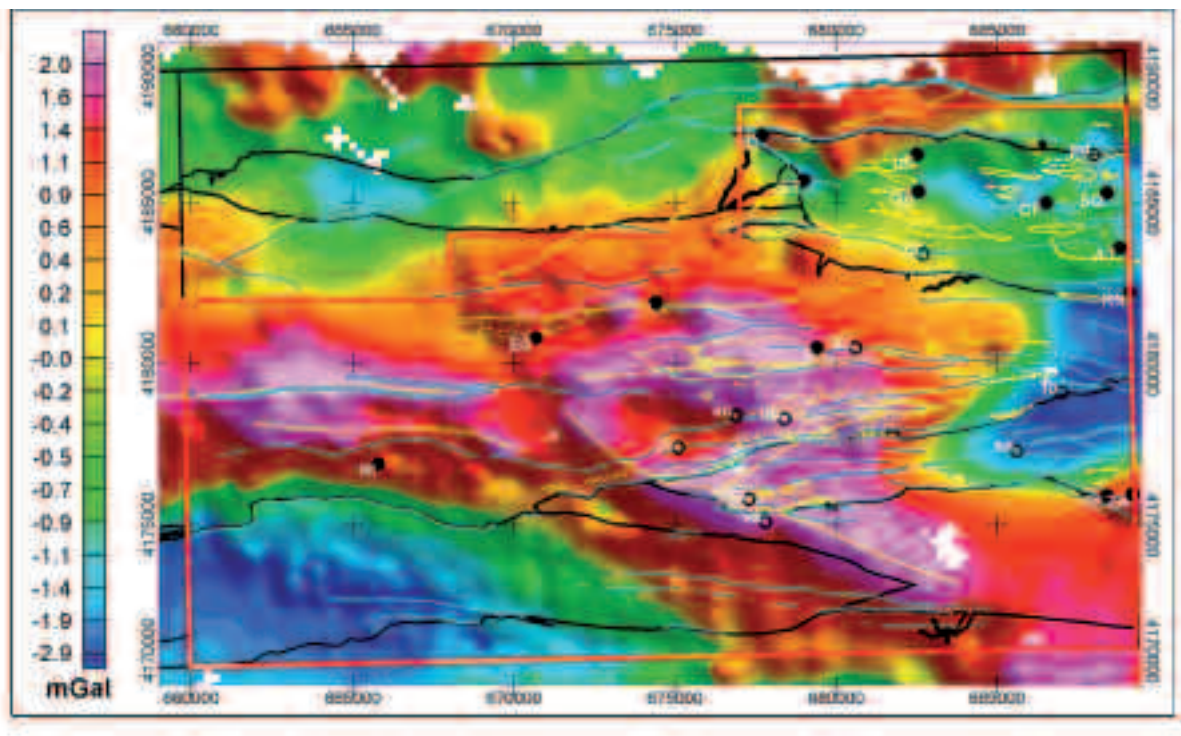

Figure 4. Residual Bouguer anomaly (topographic sheet 937). Black lines: main tectonic units. Dashed yellow lines: mafic volcanites. Cyan lines: shear bands. Yellow lines: gravity anomaly axis. Black dots: massive sulphide deposits. Circles: Manganese deposits. Deposit labels in white (names in Table IV)

Figura 4. Anomalía de Bouguer residual (hoja topográfica 937). Líneas en negro: principales unidades tectónicas. Líneas amarillas discontinuas: volcanitas máficas. Líneas cyan: bandas de cizalla. Líneas amarillas: ejes de anomalías gravimétricas. Círculos negros: depósitos de sulfuros masivos. Círculos abiertos: depósitos de manganeso. En blanco: etiquetas de los depósitos (nombres en Tabla IV)

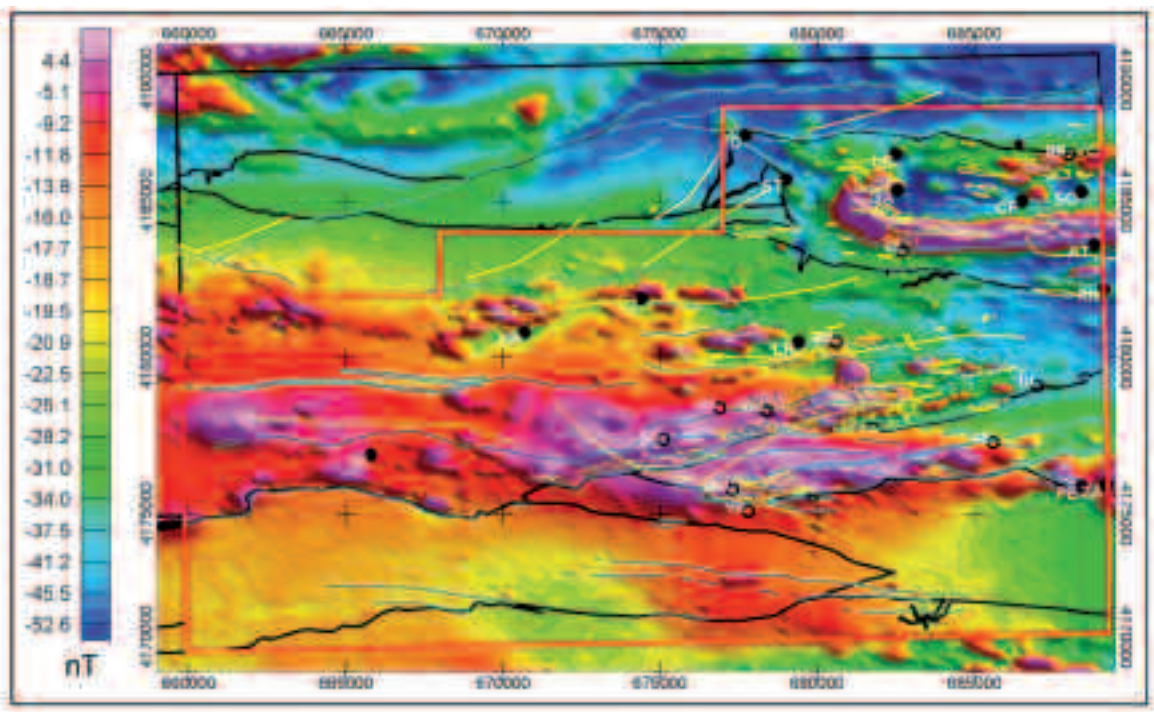

Figure 5. Reduced to pole total magnetic field (topographic sheet 937). Black lines: main tectonic units. Dashed yellow lines: mafic volcanites. Cyan lines: shear bands. Yellow lines: gravity anomaly axis. Black dots: massive sulphide deposits. Circles: Manganese deposits. Deposit labels in white (names in Table IV)

Figura 5. Campo total reducido al polo (hoja topográfica 937). Líneas en negro: principales unidades tectónicas. Líneas amarillas discontinuas: volcanitas máficas. Líneas cyan: bandas de cizalla. Líneas amarillas: ejes de anomalías gravimétricas. Círculos negros: depósitos de sulfuros masivos. Círculos abiertos: depósitos de manganeso. En blanco: etiquetas de los depósitos (nombres en Tabla IV)

and over metasedimentary ones of Duque and Gafo Units. Maxima in the central area of Gibraltar-Panera Unit and south of it are caused by VSC intermediate-mafic volcanites.

The reduced to pole total magnetic field (Figure 5) maps very well the different magnetic character of volcanic versus metasedimentary rocks. This field is characterised by a superposition of E-W anomaly bands of different wavelength. Broader maxima are located over the Gibraltar-Panera and Río Tinto-Nerva Units, with several narrower and more intense bands of maxima on top, which delineate either structural limits and/or elongated outcrops of mafic volcanites. An arcuated band of prominent maxima is spatially coincident with the long wavelength gravity minimum that characterises Concepción Unit. Magnetic anomalies constitute a good tool for mapping the ferromagnetic basic materials, clearly suggesting the full extension of basaltic-diabase sills and jasper occurrences only partially represented in the geological map. Paramagnetic felsic volcanites and metasedimentary materials produce magnetic lows.

As measured gravity data points are spaced some 0.5-1.0 km, and grid cell size is 0.5 km, vertical derivative of the residual Bouguer anomaly contains short wavelength (less than 4 km) anomalous responses either from near surface mafic volcanic axes or from not very deep buried bodies that may have mining interest (Figure 6). In the latter case we can observe that some maxima of wavelengths around or less than 2 km are associated to known mineral deposits.

The vertical derivative of the reduced to pole total magnetic field shows a good correlation with main basic volcanic outcroppings, structural limits and shear zones (Figure 7). This image is more difficult to interpret in terms of local anomalies of mining interest, due to the masking effect of mafic volcanics that produce responses of wavelength greater than 2 km.

Most of the massive sulphide occurrences (9 out of 14) are located in areas of vertical gradient gravity anomalies (taking as anomalous threshold the mean plus one standard deviation of the gradient grid, equal to 0.0011 mGal/m). In the case of the magnetic vertical gradient, all the occurrences but one are loca-

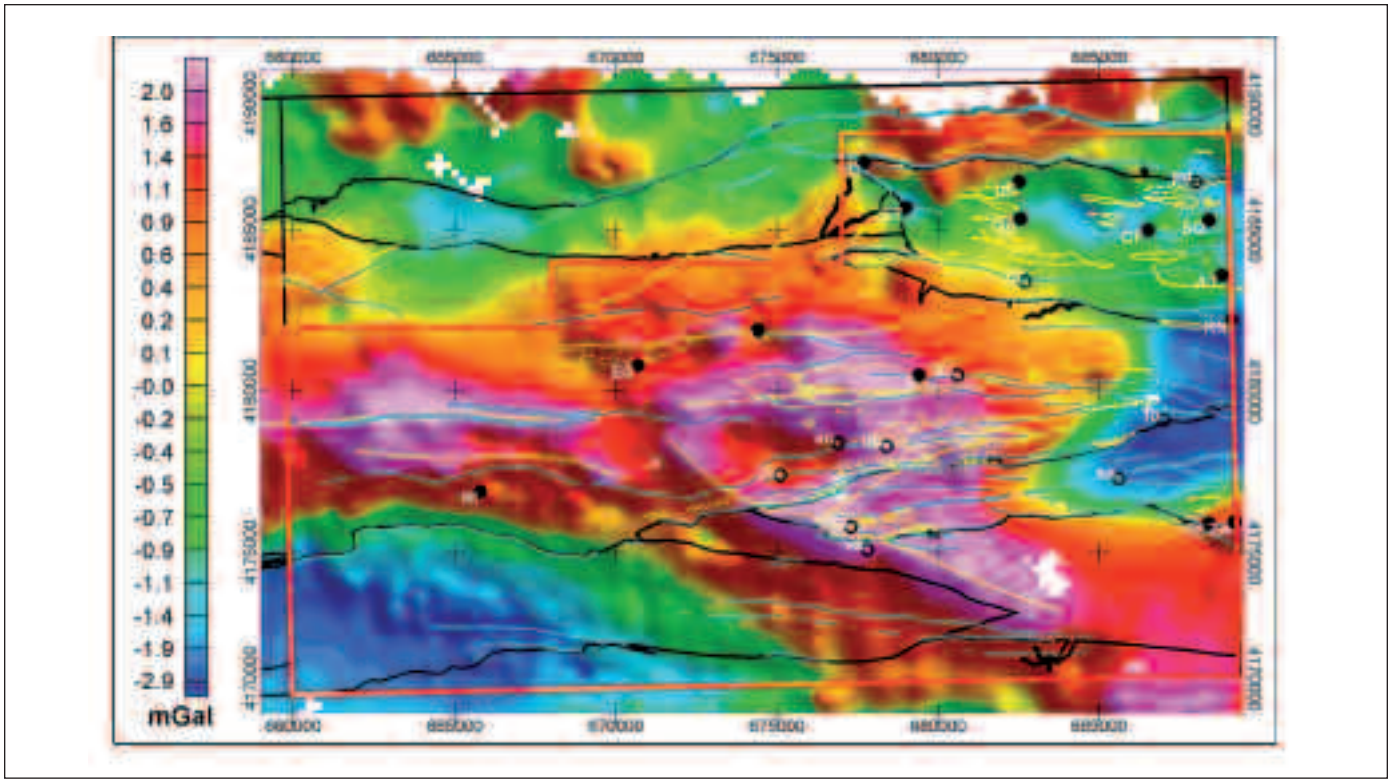

Figure 6. Vertical derivative of residual Bouguer anomaly (topographic sheet 937). Black lines: main tectonic units. Dashed yellow lines: mafic volcanites. Cyan lines: shear bands. Yellow lines: gravity anomaly axis. Black dots: massive sulphide deposits. Circles: Manganese deposits. Deposit labels in white (names in Table IV)

Figura 6. Derivada vertical de la anomalía de Bouguer residual (hoja topográfica 937). Líneas en negro: principales unidades tectónicas. Líneas amarillas discontinuas: volcanitas máficas. Líneas cyan: bandas de cizalla. Líneas amarillas: ejes de anomalías gravimétricas. Círculos negros: depósitos de sulfuros masivos. Círculos abiertos: depósitos de manganeso. En blanco: etiquetas de los depósitos (nombres en Tabla IV)

ted in anomalous zones (taking as anomalous threshold the average plus one standard deviation of the gradient grid, equal to 0.0010 nT/m; red colours in Figure 7). Nonetheless, it is difficult to establish direct relationships between potential field anomalies and the occurrences.

To analyse the radiometric location of mine occurrences, definition of maximum and minimum radiometric anomalies is made through the selection of upper and lower reference values. For instance, these reference values can be set at the "background" grid mean plus/minus 1, 2 or 3 standard deviation (two or three successive removal of the extreme values of the grid is enough to approximate the values of the average and standard deviation of the background data or "regional base"). Results are shown in Figure 3. Only three sulphide mine sites are located in zones of natural gamma radiation anomalies.

Further discussion on the interpretation of the working geophysical images and mine occurrence responses at the IPB can be found in García-Lobón and Ayala (2004), and García Lobón and Peláez Martínez (1999).

Identification of interest areas: mineral favourability mapping

The integration of geological and geophysical data is carried out with the help of a Geographical Information System and some spatial analysis extensions (Kemp *et al.*, 2001). The goal is to generate mineral favourability maps employing different data driven methods; i.e. weights of evidence, logistic regression and neural networks. Input datasets for the statistical models underwent a preprocessing, described below, after being selected from the general IPB database as indicative of the presence of VMS deposits. In all cases, lithological units and structural features (thrust belts/shear zones), as well as vertical derivatives of gravity, magnetic and radiometric grids were used as inputs, together with 22 known loca-

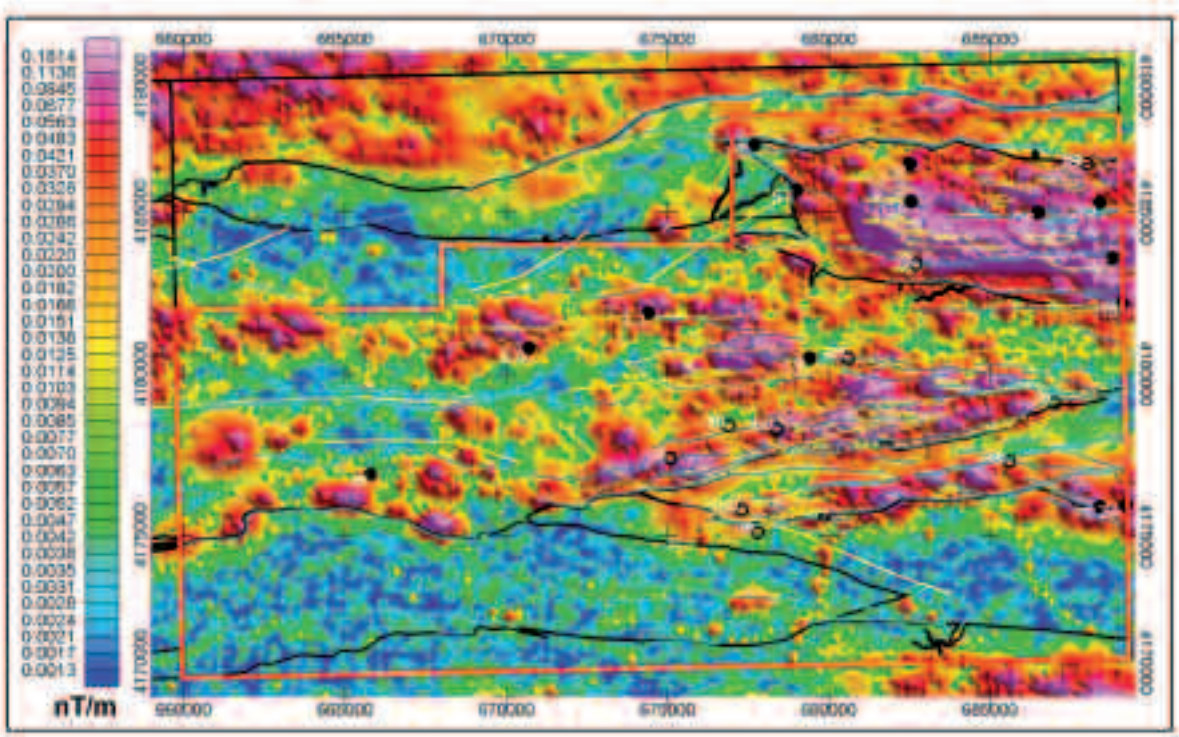

Figure 7. Vertical derivative of the reduced to pole total magnetic field (topographic sheet 937). Black lines: main tectonic units. Dashed yellow lines: mafic volcanites. Cyan lines: shear bands. Yellow lines: gravity anomaly axis. Black dots: massive sulphide deposits. Circles: Manganese deposits. Deposit labels in white (names in Table IV)

Figura 7. Derivada vertical del campo magnético total reducido al polo (hoja topográfica 937). Líneas en negro: principales unidades tectónicas. Líneas amarillas discontinuas: volcanitas máficas. Líneas cyan: bandas de cizalla. Líneas amarillas: ejes de anomalías gravimétricas. Círculos negros: depósitos de sulfuros masivos. Círculos abiertos: depósitos de manganeso. En blanco: etiquetas de los depósitos (nombres en Tabla IV)

tions of mineral deposits. A common characteristic of the three aforementioned methods is that the evidential maps/grids are first reclassified (usually categorically) and then overlaid into a unique condition map, representing the unique combination of the classes of the input maps.

Weights of Evidence and Logistic Regression

These two methods are introduced together because they involve the same input consisting of five binary evidential maps and, therefore, preprocessing is common for both.

Weights of Evidence (Wofe)

The mathematical background of this methodology is a log linear application of the Baye´s rule. Main characteristics of weights of evidence are the binary input maps and the assumption of conditional independence between maps, prerequisite which is rarely fulfilled by geophysical or geochemical data with respect to the geological/structural maps.

A parameter called weight, W (Bonham-Carter *et al.,* 1988, 1989), is initially calculated for each predictive map, as a measure of the spatial association between the presence (W^+) or absence (W^-) of the pattern (binary map) and available mineral occurrences. Consequently, a positive (W^+) and a negative (W^-) weight are calculated as log ratios of conditional probabilities for each binary evidential map:

$$W^+_i = \log(P[Bi|d]/ P[Bi|d^-]),\ W^-_i = \log(P[B^-_i|d]/ P[B^-i|d^-])$$

where d corresponds to mineral deposits (P[d]=d/total area), Bi (i=1...5) to predictive map areas; superscript k (+ or –) refers to the presence or absence of every binary pattern involved. If both weights are subtracted, the contrast C is obtained, $C = W^+ - W^-$; the higher the contrast, the stronger the spatial association. The

pairwise ¯2 test can be calculated to check if the requisite of conditional independence is violated (in case of a strong conditional dependency, the theme should be excluded of the evidential map set).

The combination of five binary evidential maps results into a set of unique conditions (with up to 2^5 classes, or feature vectors). Using Baye´s rule, a posterior probability value p,

$$p=p[d|B_1^k?B_2^k?B_3^k?B_4^k?B_5^k],$$

is calculated for each input feature vector:

$$\log(p/(1-p))=\log(P[d]/(1-P[d]))+\text{™}^5_{i=1}W^k_i$$

Logistic Regression (LR)

This method applies regression equations to evaluate the degree of correlation existing between the variables of the model. It is a log linear method as well, and results are similar to those yielded by weights of evidence. However, no assumption of conditional independence is required between input data.

A regression analysis $Y=b_0 + b_1 X_1 + ...+ bn\,Xn$ has two main parts:

The dependent variable Y is the predictive phenomenon. In our case it refers to deposit occurrences.

The independent variables X_1...Xn or known attributes are the evidential maps.

Correlation coefficients b_o.....bn are calculated for every evidential map. These coefficients quantify the strength of the spatial association between inputs and mineral deposits. As a result, binary predictor themes can be arranged decreasingly according to its spatial association with mineral deposits. In our case the order is: shear zones, magnetic and gravity fields (vertical derivatives), lithology and radiometric images. Finally, posterior probability values are calculated for the unique conditions obtaining the favourability map:

$$\log\,(p/1-p)=b_0 + b_1 X_1 + ...+ bn\,Xn$$

Model generation

The five predictive maps selected for the application of Wofe and LR in the in the Northwestern Domain of IPB were reclassified into binary maps following the criteria of maximizing the contrast, to assure the strongest spatial association between binary maps and training points (known mine sites). Several trials were carried out to obtain the binary maps. For example, shear zones (available in digitized form from the geological MAGNA 1:25,000 series) were successively buffered at distances of 100, 150, 200, 250 and 300 m. After calculation of contrasts C, it was concluded that the 100 m buffer distance maximized this parameter; so it was selected as the shear band predictive binary map (100 m buffer area = class 2, rest of the map = class 1). Criteria applied for preparing the binary lithology map (digital MAGNA 937, 1:50,000 sheet) were: class 2 = presence of VSC rocks, class 1 = VSC absent. For vertical derivatives of the geophysical grids, criteria were: class 2 = grid values > mean + 1 standard deviation, class 1 = rest of grid. The binary maps resulting of this process were used to calculate the posterior probability values using Wofe and LR mathematics.

Neural network method (RBFLN algorithm)

Artificial neural networks can be classified in two main sets concerning the type of training: in the unsupervised training the neural network learns by statistical patterns intrinsic to the data; supervised training means that the neural network learns by examples of input data where the characteristic parameter (presence or absence of mineral deposits) is known.

In this study we have selected a supervised training algorithm called radial basis functional link net (RBFLN) already used for mineral resources assessment in several works (e.g. Looney, 2002; Porwall *et al.*, 2003; Behnia and Deren, 2005). This feedforward network has a three-layer structure comprising the input, hidden and output layers. Each node of the hidden layer, also called neuron, is a radial basis function (RBF) which is a Gaussian function with a center vector v and a spread parameter σ that processes any input vector x by (Figure 8)

$$y=f(x, v)=e^{[-\|x-v\|^2/2\hat{U}^2]}$$

The name *radial* indicates that all points x equidistant from v yield the same value y. The network is trained by an back-propagation error processing with a number of deposit and non deposit training vectors x_i, which means an iterative adjustment until the weights at the neurons (u_{mj}, w_{nj}) force the outputs z to approximate their targets t very closely. This is mathematically represented by minimizing the total sum of squared error

$$E=\text{™}_{(q=1,Q)}\ \text{™}_{(j=1,J)}(t_j^q - z_j^q)^2$$

Outputs are obtained by

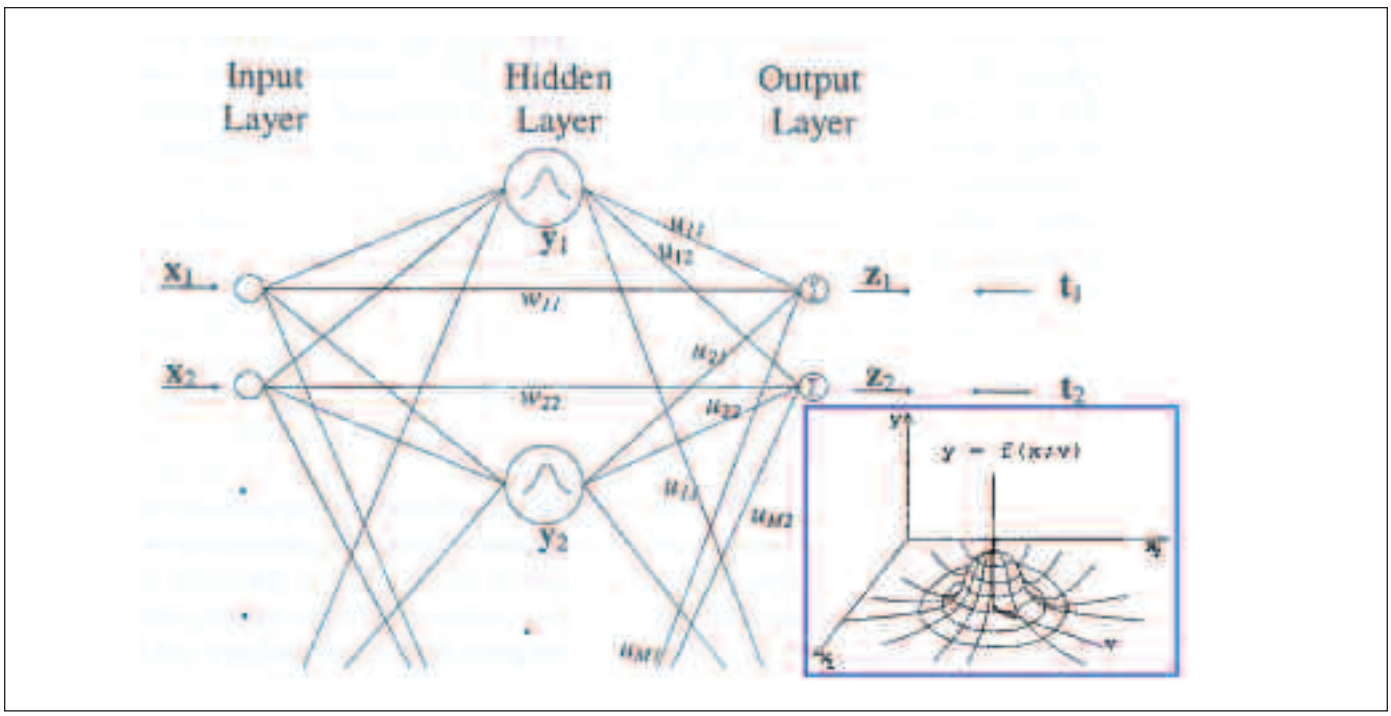

Figure 8. Radial basis functional link net (RBFLN), with a perspective of a radial basis function (RBF) in a two-dimensional feature space (after Porwall *et al.,* 2003)

Figura 8. Red neuronal de funciones de base radial (RBFLN), con una perspectiva de las funciones radiales de base (RBF) en un espacio de dos dimensiones (redibujado de Porwall y otros, 2003)

$$z_j^q = [1/(M+N)]\{[\text{TM}^N{}_1 u_{mj} y_m^q][\text{TM}^M{}_1 w_{nj} x_n^q + bj]\}$$

(Porwall *et al.*, 2003).

This data-driven approach uses both, presence and absence of mineral deposits, attempting to discover the association between map predictors and the actual response map. Data on negative associations are often poorly documented; therefore the generation of non deposit training points has been a matter of discussion. In our case, non deposits were randomly generated following the instructions of ArcSDM manual (Kemp *et al.*, 2001), i.e. in those areas of posterior probability lower than the prior probability on the weights of evidence final map.

Preprocessing of data

The lithological map (digitized geological map MAGNA 1:50.000 scale) was synthesized to highlight those rocks of the VSC that host the mineral deposits from the metasedimentary rocks. A five classes evidential map was obtained (felsic VSC, mafic VSC, intermediate VSC, epiclastic VSC and metasedimentary rocks). Shear zones were selected as principal tectonic markers, indicative of mineral occurrences. Two different buffer distances were considered: 100 m for those shear zones within the VSC and 200 m for those located over metasedimentary rocks, resulting a three classes evidential map. As in the case of Wofe and LR methods, the geophysical data selected as predictive maps were the vertical derivatives of the residual Bouguer anomaly, the total magnetic field and the potassium radiometric grid. They were classified by the grid standard deviation and lately reclassified into three classes to conform the evidential maps (values under the grid mean + 1 standard deviation; values between the mean + 1 std. dev. and mean + 2 std. dev.; and values over mean plus 2 std. deviations).

Model generation

The process for generating the RBFLN model follows three steps:

a) Training: feature vectors resulting from the overlay of the five evidential maps and 44 training points (22 deposits and 22 non deposits), were used to feed the RBFLN while training.

In the general methodology, the set of training vectors $\mathbf{x}_i$ is assigned to a binary target output to indicate the presence of deposits (1) or non deposits (0). This means that training vectors labelled as 1, can be randomly divided in two subsets: training and testing sets. Training vectors labelled as 0 can also be divided into a training and a testing set. Masters (1993) recommends the use of three sets (deposit training and testing, non-deposit training) to avoid overlearning. In this study we have employed three sets due to the small number of available deposit vectors.

*b) Test: w*hen the procedure is effective, training parameters are applied to the testing set, to validate the network behaviour.

c) Classify: after training, the network recognises the presence or absence of mineral deposits and as a result it can be used for classifying the whole feature vector space (of 274 elements in our case). The classification sum of squared error (SSE) depends on how well deposits and non deposits are distributed along the study area (Behnia and Deren, 2005).

Results

The three employed methods offer results of similar pattern. This can be observed in the Figure 9 where all histograms have a 3-fold mode, close to posterior probabilities of 0.02, 0.16 and 0.4 for Wofe; 3%, 16% and 22% for LR; and predictive classification (pattern membership) values of 0.35, 0.6 and 0.9 in the case of RBFLN.

Values exceeding the highest modes can be interpreted as representing the most favourable areas in each case (some 5%, 4%, and 5% of the total area for Wofe, LR and RBFLN, respectively).

Wofe and LR spatial association values fall within usual ranges (Bonham-Carter *et al*., 1988, 1989) (contrast $C = W^+ - W^-$ is only low in the case of the potassium grid, Table II).

Table III shows the feature vectors of highest probability (there are 31 different spatial combinations between the binary maps): data are ordered by Wofe_Posterior_Probability value. The columns appear from right to left with diminishing significance for highest Wofe results (from binary buffered shear zones to binary potassium grid values, through magnetics, gravity and geology). Wofe values higher than 0.37 represents 5.7% of the total analysed area; LR values higher than 0.23 represents the 4.03%.

Predictive maps with the distribution of posterior probabilities are shown in Figure 10.

Wofe and LR results are favoured by the occurrence of VSC rocks (Figure 10), which, as expected, are very well mapped by the two methods (the VSC corresponds with intermediate through high favourability values). Areas of felsic VSC displaying potential field anomalies are highlighted by both, Wofe and LR, especially in the case of Concepción Unit (upper-right corner Unit in figures 1 and 10, with the highest mine site concentration, where mining research programs are still being run). However, some differences can be observed: maximum Wofe values appear over central shear zones of Concepción Unit, while LR maxima appear aside these bands.

Within intermediate and mafic VSC rocks of

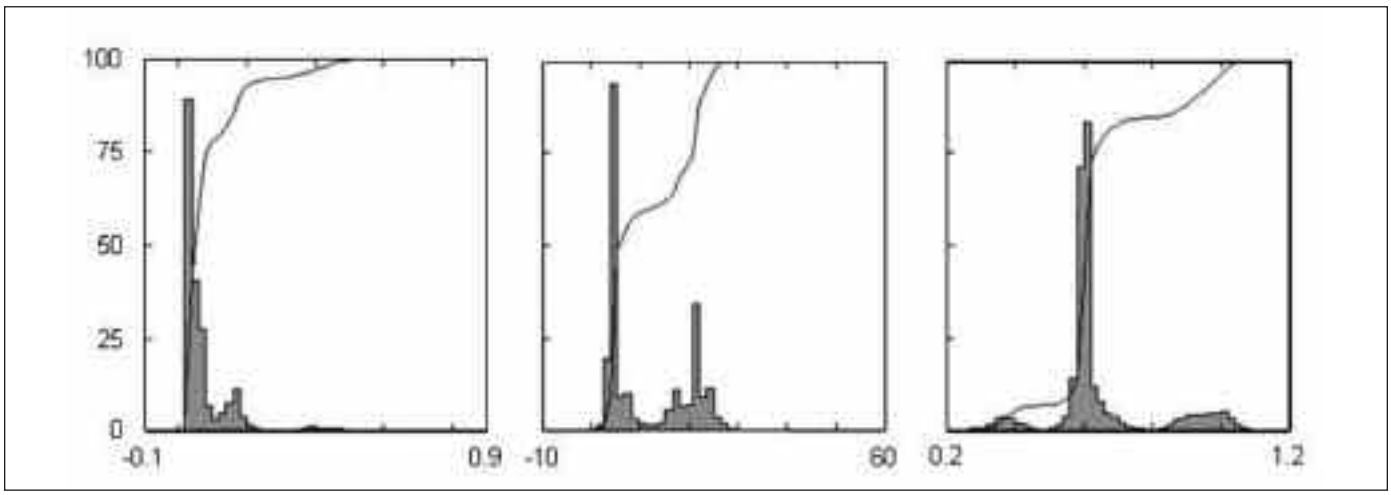

Figure 9. Left to right: Wofe, LR and RBFLN histograms
Figura 9. De derecha a izquierda: histogramas correspondientes a Wofe, LR y RBFLN

	Weights of Evidence	**Logistic Regression**
Evidential theme	*Contrast*	*Coefficient*
Shear bands	1,564	1,285
Magnetic	1,556	0,880
Gravity	1,238	0,876
Lithology	1,112	0,599
Potassium	0,544	0,327

Table II. Theme spatial association (Wofe and LR methods)
Tabla II. Asociación espacial de los temas (métodos: Peso de las Evidencias, Wofe, y Regresión Logística, LR)

Count	Unique conditions					AREA	Wofe_Post_	LR_Post_
	Shear bands	Magnetics	Gravity	Geology	Potassium	(Km^2)	Prob	Prob
21	2	2	2	2	2	0.21	0,784	0,422
236	2	2	2	2	1	2.36	0,740	0,429
2	2	2	2	1	2	0.02	0,544	0,286
102	2	2	1	2	2	1.02	0,513	0,233
33	2	2	2	1	1	0.33	0,483	0,292
862	2	2	1	2	1	8.62	0,452	0,238
26	2	1	2	2	2	0.26	0,434	0,232
52	1	2	2	2	2	0.52	0,432	0,168
421	2	1	2	2	1	4.21	0,375	0,237
610	1	2	2	2	1	6.10	0,373	0,171
39	2	2	1	1	2	0.39	0,257	0,143

Table III. Unique conditions (feature vectors) of highest probability (Wofe and LR methods). Total study area≅420 km^2 (cell size=100 m)
Tabla III. Vectores de condiciones únicas de mayor probabilidad (métodos Wofe y LR). Área total estudiada≅420 km^2 (tamaño de celda =100 m)

Gibraltar-Panera Unit (central Unit limited by thrust belts that spans over a half of the analysed area, Figures 1 and 10) there are also some differences: Wofe tends to highlight shear zones, with maximum values close to very intense residual potential trends (yellow tones in Figure 10) on the South-East border of the Unit; LR highights some aspects of these trends, but also another one over a well-known mafic volcanic axes that produce clear magnetic anomalies and encompasses two notorious mines, namely El Risquillo and La Joya (ER and LJ in the central upper part of Gibraltar-Panera Unit, Figure 10). Shear zones weigh less in LR than in Wofe in felsic/mafic VSC lithologies; the opposite occurs in metasedimentary units, in the sense of lesser favourability.

The output of the RBFLN model is the predictive classification map (Figure 10, lower image) defining several classes of RBFLN pattern membership. Results are fully dominated by shear zones (Table II): 15 out of 22 mine sites are located over shear zones and get classification values higher than 0.87. The interpretation of the RBFLN model is then straightforward: values between 0.3-0.4 correspond to shear zones without mines on them (metasedimentary areas), values close to 0.9 correspond to shear zones with mines on them and intermediate results close to

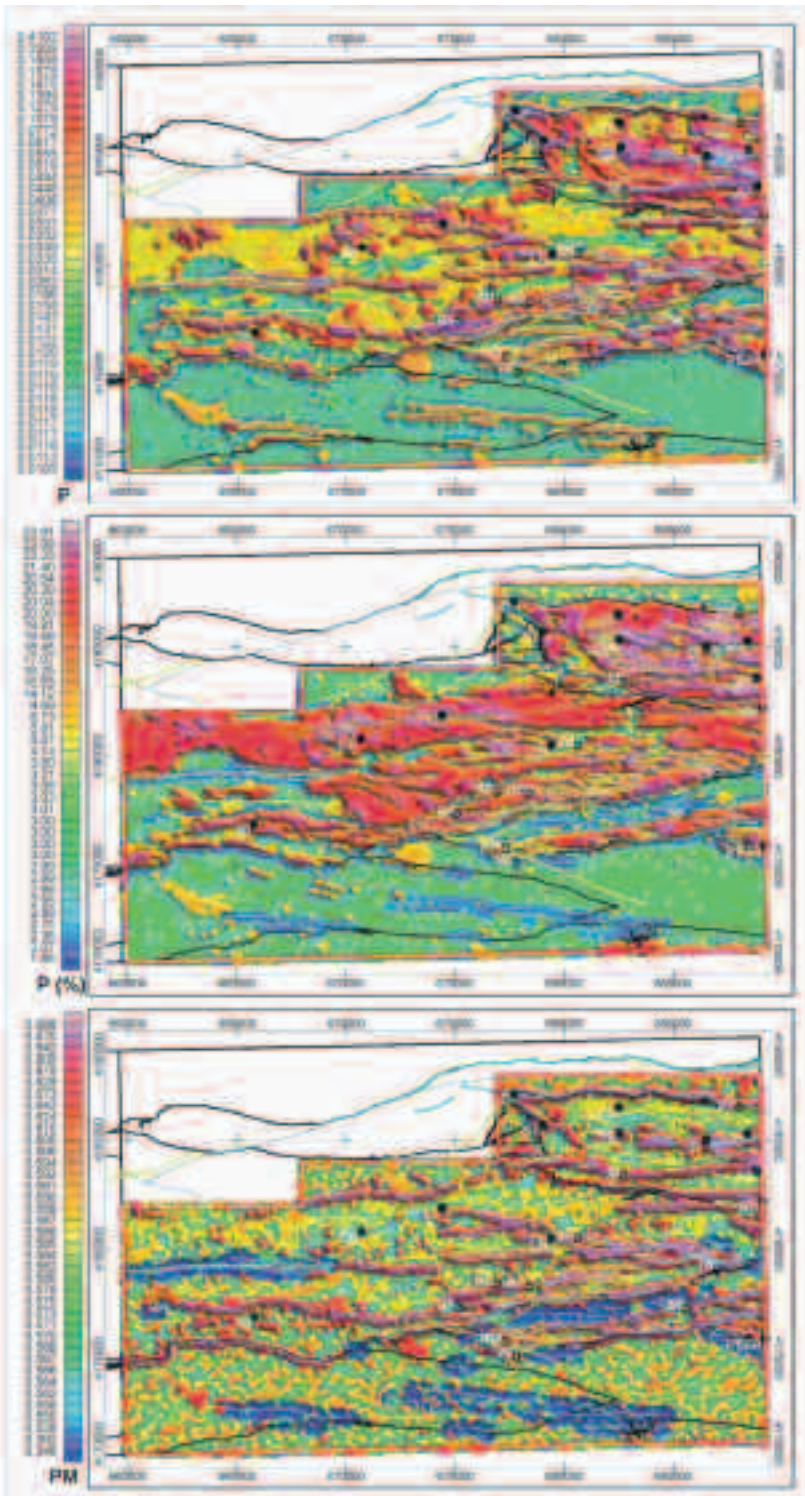

Figure 10. Wofe (upper image), LR (middle image) and RBFLN (lower image) results. Topographic sheet 937. Black lines: main tectonic units. Dashed yellow lines: mafic volcanites. Cyan lines: shear bands. Yellow lines: gravity anomaly axis. Black dots: massive sulphide deposits. Circles: Manganese deposits. Deposit labels in white (names in Table IV)

Figura 10. Resultados correspondientes a Wofe (imagen superior), LR (imagen central) y RBFLN (imagen inferior). Hoja topográfica 937. Líneas en negro: principales unidades tectónicas. Líneas amarillas discontinuas: volcanitas máficas. Líneas cyan: bandas de cizalla. Líneas amarillas: ejes de anomalías gravimétricas. Círculos negros: depósitos de sulfuros masivos. Círculos abiertos: depósitos de manganeso. En blanco: etiquetas de los depósitos (nombres en Tabla IV)

X_UTM	Y_UTM	SITE	C	Su	Un	SB	G	M	ET	W_PPr	LR_PPr	RbfIn_PM
688800	4183600	Aguas Teñidas	Ep	S	CO	x	x	x	AT	0.740	0.429	0.988
689200	4175950	La Zarza	Ep	S	RT	x	x	x	ZA	0.740	0.429	1.016
688400	4175900	Perrunal	Ep	S	RT	x	x	x	PE	0.740	0.429	0.913
679000	4185700	San Telmo	Ep	S	CO	x	x	x	ST	0.165	0.145	0.988
674400	4181900	La Joya	Vb	S	GP	x	x	x	LJ	0.373	0.171	0.975
682500	4186500	Lomero-Poyatos	FA	S	CO	-	-	x	LP	0.147	0.079	0.586
689100	4182200	Romanita	Ep	S	CO	x	-	x	RN	0.513	0.233	0.879
686500	4185000	Confesionarios	Ep	S	CO	x	x	x	CF	0.375	0.237	0.988
688400	4185300	Sorpresa	Ep	S	CO	x	x	x	SO	0.111	0.079	0.976
670700	4180800	El Risquillo	FA	S	GP	-	-	x	ER	0.035	0.034	0.562
665800	4176900	La Rica	Ep	S	GP	-	x	x	RI	0.011	0.019	0.564
682550	4185350	La Gallega	Ep	S	CO	x	x	x	GA	0.452	0.238	0.873
677700	4187100	El Carpio	Ep	S	CO	x	-	x	EC	0.148	0.114	0.881
679400	4180500	Lancha-Roma	Ep	S	GP	x	-	x	LR	0.148	0.114	0.995
682700	4183400	Cicerón	Pz	Mn	CO	x	x	x	ci	0,452	0,238	0,988
688000	4186500	Palomera	Pz	Mn	CO	x	-	x	pa	0,182	0,112	0,979
678400	4178300	Bodegón	Ep	Mn	GP	-	-	x	bo	0,147	0,079	0,582
680600	4180500	Adelfitas	Pz	Mn	GP	x	x	x	ad	0,054	0,066	0,882
675100	4177400	Guerra	Ep	Mn	GP	-	x	x	fo	0,375	0,237	0,556
687000	4179100	Fontanilla	Pz	Mn	GP	x	-	-	fo	0,054	0,066	1,028
676900	4178400	Ángel	Pz	Mn	GP	-	-	x	an	0,012	0,019	0,591
677300	4175800	Madroñosa	Vb	Mn	RT	-	-	x	ma	0,147	0,079	0,590

Table IV. Characteristics of mine sites used within the data driven methods framework. C: host rock (felsic epiclastites, Ep; shales, Pz; mafic volcanites Vb; Andesitic Fm., FA). Su: ore type (S: sulphides, Mn: manganese). Un: tectonic unit (CO Concepción, GP Gibraltar-Panera, RT Río Tinto). SB: mine site associated to shear band (11 out of 14 VMS sites; 4 out of 8 Mn sites). G/M: occurrence of gravimetric/ magnetic vertical gradient anomaly (site values> grid mean + 1 std dev). ET: deposit label in figures 4, 5, etc. W_PPr, LR_PPr : posterior probabilities for Weights of Evidence and Logistic Regression. RbfIn_PM: RBFLN pattern membership value

Tabla IV. Características de las minas utilizadas en los métodos estudiados. C: roca encajante (epiclastitas félsicas, Ep; pizarras, Pz; volcanitas máficas, Vb; Formación Andesítica, FA). Su: sustancia (S: sulfuros; Mn: manganeso). Un: unidad tectónica (CO: Concepción; GP: Gibraltar-Panera, RT: Río Tinto). SB: mina asociada a banda de cizalla (11 de catorce depósitos de sulfuros masivos; 4 de 8 depósitos de manganeso). G/M: anomalía de gradiente vertical gravimétrico/magnético (valores > media de la malla + 1 desv. std.). ET: etiquetas de los depósitos correspondientes a las figuras 4, 5, 6, 7, 10. W_PPr, LR_PPr: probabilidades a posteriori para los métodos Pesos de las Evidencias (Wofe) y Regresión Logística (LR). Rbfln_P: clasificación predictiva para el método Red neuronal de funciones de bases radiales (RBFLN)

0.6 represent indifferent areas. These facts are irrespective of the mine situation within the potential field anomalies; VSC outcrops or potential field anomaly axes do not influence RBFLN results.

Table IV presents mineral deposits and their geophysical and algorithmic method responses.

Table IV shows that in the case of VMS deposits, 64% of the mineral deposits are located in gravity

anomaly areas, 100% in magnetic anomaly areas, and 50% in high favourability areas of the mineral potential map for Wofe and LR, and 79% for RBFLN.

In summary, most favourable zones defined by the used algorithmic mapping methods (Wofe, LR and RBFLN) amount to a similar percentage of the total investigated area (5%). In the case of RBFLN models, these most prospective zones strictly coincide with structural boundaries, thrust or shear zones. In the case of Wofe and LR models, favourable zones are directly related to these limits where they produce potential field anomalies. Consequently, areas close to shear zones in felsic VSC are highlighted by the latter, especially in the case of Concepción Unit, where potential anomalies are abundant. Outside felsic areas, some volcanic axes show enhanced Wofe and LR results. At the opposite extreme, most unfavourable zones correspond to shear zones in metasedimentary areas.

Conclusions

Main geophysical conclusions can be summarized as follows:

1) Structural imbrication of igneous (felsic-mafic) and metasedimentary units originates the recorded anomalous responses of potential fields (Figures 4 and 5). High resolution gravity and magnetic mapping in the NW domain of the IPB constitutes an excellent example of the advantage of using potential fields to map volcanic areas.

2) Potential field data provide clear evidence of the relationship between mineral deposits and structural boundaries (thrust or shear zones), within whose vicinity the former take place in most of cases.

3) In the NW domain of the IPB, high amplitude (tens to hundreds of nT and 1-3 mGal) long (λ>4 km) and intermediate (4 km>λ>2 km) wavelength magnetic and gravimetric anomalies can be mainly attributed to basaltic or intermediate rocks (the latter, with only gravity effects). Most of volcanic massive sulphide deposits appear over anomalous potential field areas of complex origin, where long and intermediate wavelength anomalies mask local responses (of few tens of nT and 0.5-1 mGal).

4) The most conspicuous short wavelength magnetic and gravimetric anomalies (λ<2 km; anomalies isolated by means of wavelength filtering) take place along the gravity axis originated from mafic volcanites and structural axes of the area. Gravity filtered images contain important families of short wavelength anomalies less related to mafic volcanites and structural bands than magnetic images. Ferromagnetic jaspers of CVS produce high amplitude, short wavelength magnetic anomalies that point out the occurrence of highly prospective volcanic and epiclastic rocks under the sedimentary cover.

5) A remarkable feature of radiometric data refers to extreme values, with spectacular potassifications occurring in rhyolites and acid tuffs located close to thrust limits and shear zones, that clearly control them.

6 A compact set of physical properties is now available for the geological interpretation of airborne and ground surveys in a characteristic mining area. The petrophysical database constitutes an outstanding reference for any study and modelling of the rocks in the NW Domain of IPB by means of natural gamma radiation and potential fields.

Concerning the combined use of favourability mapping techniques and geophysical images, the main conclusions are:

1) Results of predictive mapping methods (Wofe, LR and RBFLN) reflect the fact that most of the deposits (70 %) are structurally controlled by thrust or shear zones, so these structural boundaries are the prospective areas highlighted by all the algorithmic methods we have employed. This does not add very much to what is already known in the study area. As the methods are data driven, based on deposit and non deposit training points, some inconveniences must be borne in mind, as the criterion of generating non-deposits in the RBFLN method (based on the posterior probability obtained by Wofe), or the number and quality distribution of available mine sites (a reduced number of deposit locations in the feature space could imply overfitting, that seems to have been the case of RBFLN results).

2) Away from structural boundaries, the spatial association of the used themes with respect to the training points can be described as moderate. Some Wofe and LR results, enlarging the influence area of some well-known mineralized axes, offer more interesting details than RBFLNs. The validations of the models are acceptable: in the final maps more than a half of the VMS deposits can be found in areas of high favourability.

3) Geophysical responses, especially magnetic ones, are not selective enough as to characterise mine areas when the structural control is absent. The spatial association between geophysical anomalies and mine sites could be improved by airborne resistivity coverages, but these are not yet available in the study area.

4) Radiometric images (total counts, potassium, and thorium) are not useful inputs to feed the neural, Wofe and LR systems. Radiometric high spots (potas-

sium, thorium) do not show a close spatial relation to mineral occurrences. However, ultrapotassifications constitute a good guide of VMS deposit prospectivity as they indicate fertile shear zones.

Acknowledgements

The present work is a contribution to a regional project on massive sulphides search in the NW Domain of the Iberian Pyrite Belt carried out by an IGME working group during 2002-2005, coordinated by Alejandro Sánchez, to whom we are in debt. Cecilio Quesada, Félix Bellido and Pablo Gumiel are thanked for their thoughtful comments and valuable contributions, which have helped to improve this paper.

References

Bates, M. y García Lobón, J. L. (1998). *Exploración aeromagnética y radiométrica de la Faja Pirítica y zonas limítrofes*. Fondo documental del IGME, Informe 40464. Madrid.

Behnia, P.; and Deren, L., 2005. Application of Radial Basis Functional Link Networks to Mineral Potential Mapping of Proterozoic Mineralization in Saghand-Chadormalu Area, Central Iran. *Proceedings of IAMG´05*, 1, 523-528

Bonham-Carter, G. F., Agterberg, F. P., and Wright, D. F., 1988. Integration of Geological Datasets for Gold Exploration in Nova Scotia. *Photogrammettry and Remote Sensing*, 54, 1585-1592.

Bonham-Carter, G. F., Agterberg, F. P., and Wright, D. F., 1989. Weights of evidence modelling: a new approach to mapping mineral potential. *Geological Survey of Canada, Paper 89-9*, 171-183.

Chiozzi, P., Pasquale, V., y Verdoya, M., 1998. Ground radiometric survey of U, Th y K on the Lipari Island, Italy. *Journal of Applied Geophysics*, 38: 209-217.

Exploranium (1998). *GR-320. Portable gamma ray spectrometer users manual*. 73 p.

García Lobón, J. L., y Peláez Martínez, A. (1999). Cartografía geofísica y situación de indicios mineros respecto de anomalías magnéticas, radiométricas y gravimétricas en cuatro áreas de la Faja Pirítica. *Boletín Geológico y Minero*, 110 (6): 715-738.

García-Lobón, J.L. and Ayala, C., 2004, Petrofísica, Aeromagnetismo, Radiometría y Gravimetría: Exploración Regional y Delimitación de Zonas Anómalas en el Dominio Noroccidental de la Faja Pirírica. *IGME Technical Report 589 (In Spanish)*. CD-Rom 157

Gumiel Martínez, P. y Mirete Mayo, S., 1999. Los yacimientos de sulfuros de la Faja Pirítica. *Colección Patrimonio Geológico De Andalucía*, pp. 224-229, ISBN: 84-931224-0-8

Junta de Andalucía, 2002. *Proyecto de Investigación Geológica y Cartografía Básica en la Faja Pirítica y Áreas Aledañas. 1998-2000.*

Kemp, L.D., Bonham-Carter,G.F., Raines,G.L., and Looney, C.G., 2001. Arc-SDM: Arc-View extension for spatial data modelling using weights of evidence, logistic regression, fuzzy logic and neural network analysis, *http://netserv.gis.nrcan.gc.ca/sdm/.*

Leistel, E. Marcoux, D. Thiéblemont, C. Quesada, A. Sánchez, G. R. Almodóvar, E. Pascual and R. Sáez., 1997. The volcanic-hosted massive sulphide deposits of the Iberian Pyrite Belt. *Journal Mineralium Deposita*. Issue Volume 33, Numbers 1-2

Looney, C. G., 2002, Radial basis functional link nets and fuzzy reasoning. *Neurocomputing*, 43, 489-509.

Masters, T. 1993. *Practical neural network recipes in C++*. Academic Press, Inc. 493 p.

Porwal, A., Carranza, E.J.M., and Hale, M., 2003, Artificial Neural networks for mineral-potential mapping: A case study from Aravalli province, western India. *Natural resources research*, 12 (3), 155-171

Recibido: mayo 2006
Aceptado: febrero 2007